This article has been accepted for publication in a future issue of this journal, but has not been fully edited. Content may change prior to final publication. Citation information: DOI 10.1109/TCSII.2018.2878188, IEEE Transactions on Circuits and Systems II: Express Briefs

Stability Analysis of Single-Phase Low-Voltage AC Microgrids with Constant Power Terminals

O. D. Montoya*, *Member, IEEE*, A. Garces†, *Senior Member, IEEE*, S. Avila-Becerril‡, G. Espinosa-Pérez‡ and F. M. Serra§

***Abstract*—This express brief presents the stability analysis of single-phase microgrids (SP-MG) operating under master–slave connection with constant power terminals. The SP-MG is composed of linear elements, nonlinear loads, and distributed generators modeled as PQ constant terminals interconnected through power electronic converters. Lyapunov's direct method through a Hamiltonian representation of the grid is used to demonstrate stability. The non-autonomous model of the SP-MG is transformed into an autonomous equivalent model based on the dynamics of the error. The proposed analysis shows that if there is an admissible trajectory $x^\star$ solution of the power flow equations, then the SP-MG is stable in the sense of Lyapunov.**

***Index Terms*—Hamiltonian systems, Lyapunov's direct method, stability analysis, single-phase microgrids.**

I. Introduction

MICROGRIDS are increasingly common in modern distribution grids: they allow efficient integration of multiple components, such as renewable generation, energy storage, and controllable loads [1], [2]. All these components require a power electronic converter for accurate control of active and reactive power. Therefore, the dynamics of the circuit become non-linear and makes stability analysis a challenging problem [3]. Microgrids can be ac or dc [4]. The former can be subclassified into three-phase and single-phase. In this paper, we study single-phase microgrids (SP-MG), which are popular in small power applications that include residential storage and generation, demand response, smart-cities, and rural areas [1].

Despite the growing literature on distributed controls for microgrids, most of the practical implementations use a master–slave control where the main distribution grid imposes a constant voltage and a fixed frequency, while the distributed resources synchronize to these conditions [5]. Each electronic power converter can be accurately modeled as a constant power terminal, since the details about internal control in low voltage components are generally inaccessible, considering that each converter may have a different technology. In addition, commercial converters have a fast dynamic and are designed to maintain an active and reactive power according to the requirements of the grid and/or the primary resource [6]. Therefore, a practical method for the stability analysis of a single-phase microgrid must consider a constant power model.

There are different approaches to study stability of general microgrids. A complete review of Lyapunov's indirect method for the stability analysis of common devices such as motors and dc controlled loads was presented in [7]. The authors of [8] present the stability analysis of ac three-phase reduced MG based on Popov's absolute stability criterion considering the connection of constant power loads (CPLs). In [9] general conditions to guarantee the existence of equilibrium points in ac MG with constant power loads was presented; they focus only on the particular ac–dc connections by using a Hamiltonian approach under autonomous and non-autonomous reference frames. The authors of [10] show the stability analysis of three-phase four-wire MGs for low-voltage applications using phasorial approximations, which approximates the dynamical behavior of the MG. In [11] some structural properties for stability of typical electrical circuits via Hamiltonian formulations are explored.

On the other hand, for operating single-phase converters, multiple-impedance based approaches have been proposed in the specialized literature [12]. Those controllers are mainly used for voltage and frequency control on isolated power grids [13], by emulating via converters the dynamical behavior of synchronous generators; as well as for active and reactive decoupled control for grid-connected applications [14]. It is important to mention that those approaches conventionally used Laplace transformations for analyzing and designing their controllers, which commonly focused on feedback methods with PI actions.

Unlike [8], we analyze the SP-MG connection with CPLs. We present a general dynamic model that considers all the possible devices that can be connected to an SP-MG via a general Hamiltonian model, which extends the reduced three-phase model proposed by [8] to SP-MGs operating under master–slave control strategy. Our model can be applied to radial or meshed topologies. The proposed analysis allows a unified method based on the structural properties of the components. The dynamical structure of the MG evidences its non-autonomous behavior, which implies the non-existence

This work was partially supported by the National Scholarship Program Doctorates of the Administrative Department of Science, Technology and Innovation of Colombia (COLCIENCIAS), by calling contest 727-2015. Also, part of this work were supported by DGAPA-UNAM under grants IN116516 and IA103519.

* O. D. Montoya is with the program of electric and electronic engineering, Universidad Tecnológica de Bolívar, Post Code: 131001, Cartagena, Colombia (email: o.d.montoyagiraldo@ieee.org)

† A. Garces is with the department of electric power engineering, Universidad Tecnológica de Pereira - Post Code: 660003 - Pereira, Colombia (email: alejandro.garces@utp.edu.co)

‡ S. Avila-Becerril and G. Espinosa-Pérez are with Universidad Nacional Autónoma de México - Post Code: 04510 - CDMX, Mexico (email: soavbec@comunidad.unam.mx, gerardoe@unam.mx)

§ F. M. Serra is with the Automation Control Laboratory (LCA), Universidad Nacional de San Luis - Post Code: 5730 - Villa Mercedes, San Luis, Argentina (e-mail: fserra@ieee.org)

This article has been accepted for publication in a future issue of this journal, but has not been fully edited. Content may change prior to final publication. Citation information: DOI 10.1109/TCSII.2018.2878188, IEEE Transactions on Circuits and Systems II: Express Briefs

of equilibrium points [8], [9], [11]. This situation complicates the classical stability analysis since it is not possible to use linear transformations to transform a non-autonomous system into an autonomous equivalent model [11]. Nevertheless, this complication in the model arises as an opportunity to analyze when the operative conditions in the SP-MGs guarantee a stable behavior in the sense of Lyapunov.

The mathematical model presented in this paper allows the analysis of stability properties of the SP-MG via Hamiltonian formulation by exploring the structural properties inherent in the power systems [11].

The remainder of this paper is organized as follows: Section II presents the dynamical formulation of an arbitrary SP-MP. Section III shows the stability analysis based on Lyapunov's direct method. Numerical evaluations are presented in Section IV. Finally, some concluding remarks are provided in Section V.

II. Dynamical Model of SP-MG

A. General Considerations

Consider a single-phase generic MG with linear and nonlinear loads operating under grid-connected mode as depicted in Fig. 2. Let us make the following assumptions for the SP-MG:

Assumption 1: The electrical connections among different nodes in the SP-MG are modeled by a connected graph with n external ports. Each port has the variables (v_k, i_k), $k = 1, \ldots, n-1$.

Assumption 2: There is a master–slave control. This implies that the SP-MG operates under grid-connected mode and that the grid provides the voltage profile and the fundamental frequency for the entire SP-MG.

Assumption 3: Each node has at least one electrical element connected directly to ground (electrical reference). This element corresponds to the capacitive effect between each branch (line) and ground.

Assumption 4: The PQ terminals are integrated to the SP-MG via single-phase voltage source converters [15]. Each PQ terminal may correspond to a constant power load or to a distributed energy resource (energy storage or distributed generator technology).

B. Dynamical Model of a Generic Node

Assume a CPL model for the $n-1$ nodes different from the master node, as presented in Fig. 1(a). Then, by Kirchhoff's law

$$f_k = g_k v_k + C_k \frac{d}{dt} v_k + i_k; \quad k = 2, 3, \ldots, n \tag{1}$$

where f_k corresponds to the current generated by the distributed energy resource or consumed by a nonlinear load connected at node k, and in matrix form

$$\vec{f_l} = \mathcal{G}_l \vec{v}_l + \mathcal{C}_l \frac{d}{dt} \vec{v}_l + \vec{i}_l, \tag{2}$$

where $\vec{f_l} = col(f_k) \in \mathbb{R}^{n-1}$, $\mathcal{C}_l, \mathcal{G}_l \in \mathbb{R}^{n-1 \times n-1}$ are diagonal matrices with positive elements C_k and g_k respectively. Notice that $\mathcal{G}_l$ contains the conductive effects associated to the constant resistive loads interconnected to each node and $\mathcal{C}_l$ contains all capacitive effects associated to the load nodes of the network.

C. Dynamical Model of a Generic Line

There are b electrical lines in the SP-MG, represented by internal edges of the graph, with variables (v_j, i_j), $j = 1, \ldots, b$. The lines can be modeled employing a classical Π model as depicted in Fig. 1(b), where L_j and R_j represent the series inductance and resistance parameters of the electrical conductor, while C_j represents the capacitive effect between the conductor and the electrical reference.

By applying Kirchhoff's laws to one line it follows that

$$v_m - v_n = v_j = L_j \frac{d}{dt} i_j + R_j i_j, \tag{3}$$

with v_m and v_n being the voltages in both ends of the line, which implies that v_j corresponds to the voltage drop in the j^{th} line, and i_j the current flowing through this line. This expression can be generalized for all branches in matrix form as

$$\vec{v}_\mathcal{E} = \mathcal{L}_\mathcal{E} \frac{d}{dt} \vec{i}_\mathcal{E} + \mathcal{R}_\mathcal{E} \vec{i}_\mathcal{E}, \tag{4}$$

where $\vec{v}_\mathcal{E} = col(v_j) \in \mathbb{R}^b$, $\vec{i}_\mathcal{E} = col(i_j) \in \mathbb{R}^b$, while $\mathcal{L}_\mathcal{E} = diag\{L_j\} \in \mathbb{R}^{b \times b}$ and $\mathcal{R}_\mathcal{E} = diag\{R_j\} \in \mathbb{R}^{b \times b}$ contain the inductive $L_j > 0$ and resistive $R_j > 0$ effects, respectively.

Remark 1: The capacitive effects of each branch C_j will be considered in the dynamics of the electrical nodes.

D. Line–Node Relationship

The line–node relationship is given by the Incidence matrix $[\mathcal{A}] \in \mathbb{R}^{b \times n}$ with entries equal to ± 1 depending on the incidence and the chosen current flow. Let the vector of nodal voltages be $\vec{v}_\mathcal{N} = col(v_k) \in \mathbb{R}^n$. Then

$$\vec{i}_\mathcal{N} = \mathcal{A}^T \vec{i}_\mathcal{E} \ , \ \vec{v}_\mathcal{E} = \mathcal{A} \vec{v}_\mathcal{N}. \tag{5}$$

Property 1: Due to the existence of a master node, the vector of nodal voltages and currents can be split as follows:

$$\vec{v}_\mathcal{N} = \begin{bmatrix} \vec{v}_0 \\ \vec{v}_l \end{bmatrix}, \ \vec{i}_\mathcal{N} = \begin{bmatrix} \vec{i}_0 \\ \vec{i}_l \end{bmatrix} \tag{6}$$

with $\vec{v}_0 \in \mathbb{R}$ and $\vec{i}_0 \in \mathbb{R}$ the master voltage and current, respectively, while the $\vec{v}_l, \vec{i}_l \in \mathbb{R}^{n-1}$ are the rest of the nodal voltages and currents. Under these conditions, Eq. (5) can also be rewritten as

$$\vec{v}_\mathcal{E} = \begin{bmatrix} \mathcal{A}_0 & \mathcal{A}_l \end{bmatrix} \begin{bmatrix} \vec{v}_0 \\ \vec{v}_l \end{bmatrix} = \mathcal{A}_0 \vec{v}_0 + \mathcal{A}_l \vec{v}_l \tag{7a}$$

$$\begin{bmatrix} \vec{i}_0 \\ \vec{i}_l \end{bmatrix} = \begin{bmatrix} \mathcal{A}_0^T \\ \mathcal{A}_l^T \end{bmatrix} \vec{i}_\mathcal{E} \ \Rightarrow \ \vec{i}_l = \mathcal{A}_l^T \vec{i}_\mathcal{E} \tag{7b}$$

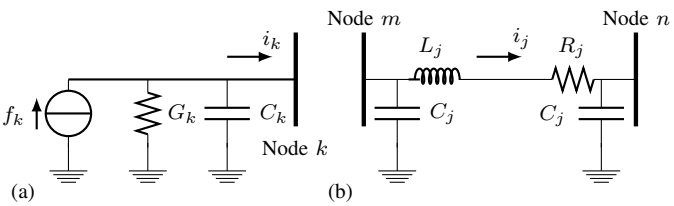

Fig. 1. π model of the j^{th} electrical branch connected between m and n nodes

This article has been accepted for publication in a future issue of this journal, but has not been fully edited. Content may change prior to final publication. Citation information: DOI 10.1109/TCSII.2018.2878188, IEEE Transactions on Circuits and Systems II: Express Briefs

with $\mathcal{A}_0 \in \mathbb{R}^{b\times 1}$ the first column of $\mathcal{A}$ and $\mathcal{A}_l \in \mathbb{R}^{b\times(n-1)}$. Eq. (7b) also implies that $\vec{i}_0 = \mathcal{A}_0^T \vec{i}_\mathcal{E}$, which is always satisfied since the master source is ideal.

E. Complete Dynamical Model

The dynamical model of the SP-MG is represented by Eqs. (4) and (2) under the line–node relation (7) as

$$\mathcal{L}_\mathcal{E} \frac{d}{dt}\vec{i}_\mathcal{E} = -\mathcal{R}_\mathcal{E}\vec{i}_\mathcal{E} + \mathcal{A}_l\vec{v}_l + \mathcal{A}_0\vec{v}_0 \tag{8a}$$

$$\mathcal{C}_l \frac{d}{dt}\vec{v}_l = -\mathcal{G}_l\vec{v}_l - \mathcal{A}_l^T\vec{i}_\mathcal{E} + \vec{f}_l \tag{8b}$$

$$\text{s.t:} \quad \vec{i}_0 = \mathcal{A}_0^T\vec{i}_\mathcal{E} \tag{8c}$$

It is important to notice that the dynamical model of the SP-MG (8) corresponds to a port-controlled Hamiltonian system with an external input

$$\mathcal{D}\dot{x} = [\mathcal{J} - \mathcal{R}]\nabla\mathcal{H}(x) + \Gamma \tag{9}$$

where $\mathcal{D} = diag\{\mathcal{L}_\mathcal{E}, \mathcal{C}_l\} \in \mathbb{R}^{(b+n-1)\times(b+n-1)}$, $\mathcal{D} = \mathcal{D}^T > 0$, the dissipation matrix $\mathcal{R} = diag\{\mathcal{R}_\mathcal{E}, G_l\} \in \mathbb{R}^{(b+n-1)\times(b+n-1)}$, $\mathcal{R} = \mathcal{R}^T > 0$, the state $x = \begin{bmatrix} \vec{i}_\mathcal{E}^T & \vec{v}_l^T \end{bmatrix}^T \in \mathbb{R}^{b+n-1}$, the matrices

$$\Gamma = \begin{bmatrix} \mathcal{A}_0\vec{v}_0 \\ \vec{f}_l \end{bmatrix} \in \mathbb{R}^{b+n-1}, \quad \mathcal{J} = \begin{bmatrix} 0 & \mathcal{A}_l \\ -\mathcal{A}_l^T & 0 \end{bmatrix} \tag{10}$$

and the quadratic function

$$\mathcal{H}(x) = \frac{1}{2}x^T x, \quad \nabla\mathcal{H}(x) = \left[\frac{\partial}{\partial x}\mathcal{H}(x)\right]^T = x \tag{11}$$

Remark 2: $\mathcal{H}(x)$ is known as the Hamiltonian function and in this case corresponds to the total energy stored in the electric and magnetic fields.

F. CPL integration through a VSC

The integration of a CPL can be made through a power VSC technology (see Fig. 2). By applying Kirchhoff's laws we obtain [15]

$$L_k \frac{d}{dt} f_k = -R_k f_k + m_k v_{dc}^k - v_k; \tag{12}$$

$$C_{dc}^k \frac{d}{dt} v_{dc}^k = i_s - m_k f_k; \tag{13}$$

where L_k and R_k are the filter inductance and resistance parameters, m_k is the averaged control input (modulation index), and v_{dc}^k corresponds to the voltage profile in the terminals of the capacitance C_{dc}^k located in the dc side of the VSC. Additionally, i_s corresponds to the current consumed by the constant power load in the dc side of the VSC.

Applying the passivity-based control theory as proposed in [11], we can control the current delivered/consumed by the distributed generator or CPL as follows:

$$m_k = \frac{1}{v_{dc}^k}\left(R_k f_k + v_k + k_p^k\left(f_k^\star - f_k\right)\right) \tag{14}$$

where $f_k^\star$ corresponds to the desired ac current reference defined as a linear function of the voltage profile v_k and the active and reactive power references $P^\star$ and $Q^\star$, i.e., $f_k^\star = \alpha P^\star v_k \pm \beta Q^\star \frac{d}{dt}v_k$.

Notice that if the control equation (14) fulfills its tasks, the current f_k enhances its desired reference, which implies that the active and reactive power consumption at the CPL terminals is controlled, and the stability behavior of the whole SP-MG is ensured [6]. For more details about the dynamical behavior of the CPLs in power systems, see [4] and [9].

III. Stability analysis

This section studies the dynamic behavior of a general SP-MG considering external sources Γ. In this sense, the admissible trajectories $x^\star(t)$ are the set of state trajectories that the system can reproduce and are the solutions of

$$\mathcal{D}\dot{x}^\star = [\mathcal{J} - \mathcal{R}]\nabla\mathcal{H}(x^\star) + \Gamma^\star \tag{15}$$

where

$$\Gamma^\star = \begin{bmatrix} \mathcal{A}_0\vec{v}_0 \\ \vec{f}_l^\star \end{bmatrix}, \text{ and } \mathcal{H}(x^\star) = \frac{1}{2}x^{\star T}x^\star$$

Define the classical tracking error as $\tilde{x} = x - x^\star$. Then the dynamic behavior for the tracking error can be written as

$$\mathcal{D}\dot{\tilde{x}} = [\mathcal{J} - \mathcal{R}]\nabla\mathcal{H}(\tilde{x}) + \tilde{\Gamma} \tag{16}$$

In the next proposition, conditions for $\tilde{x} \to 0$ are given.

Proposition 1: Assume that $\vec{v}_0(t)$ and $\vec{f}_l(t)$ are time-varying and that their steady state behaviors are well defined. Then, $\tilde{x}(t)$ of the system (16) is ultimately bounded. Moreover, if it is assumed that $\vec{f}_l^\star(t) = \vec{f}_l(t)$ is imposed by the constant power load controllers, which means $\tilde{\Gamma} \to 0$, asymptotic stability of $\tilde{x} = 0$ is achieved.

Proof: Consider the positive function

$$\mathcal{V}(\tilde{x}) = \frac{1}{2}\tilde{x}^T\mathcal{D}\tilde{x} \tag{17}$$

The time derivative of (17) along the trajectories of (16) is

$$\begin{aligned}\dot{\mathcal{V}}(\tilde{x}) &= -\tilde{x}^T\mathcal{R}\tilde{x} + \tilde{x}^T\tilde{\Gamma} \\ &\leq -\lambda_{\min}\{\mathcal{R}\}|\tilde{x}|^2 + |\tilde{x}||\tilde{\Gamma}| \\ &= -(1-\theta)\lambda_{\min}\{\mathcal{R}\}|\tilde{x}|^2 - \theta\lambda_{\min}\{\mathcal{R}\}|\tilde{x}|^2 + |\tilde{x}||\tilde{\Gamma}|\end{aligned}$$

with $0 < \theta < 1$, while $\lambda_{\min}\{\mathcal{R}\}$ stands for the minimum eigenvalue of $\mathcal{R}$ and $|\cdot|$ denotes the norm. So, it can be concluded that

$$\dot{\mathcal{V}}(\tilde{x}) \leq -(1-\theta)\lambda_{\min}\{\mathcal{R}\}|\tilde{x}|^2 \tag{18}$$

for all

$$|\tilde{x}| \geq \frac{|\tilde{\Gamma}|}{\theta\lambda_{\min}\{\mathcal{R}\}} > 0 \tag{19}$$

Since $(1-\theta)\lambda_{\min}\{\mathcal{R}\}|\tilde{x}|^2$ is a continuous positive definite function of $\tilde{x}$, inequality (18) shows that the solutions $\tilde{x}(t)$ are ultimately bounded. Moreover, notice that if it is assumed that the control of the power converters guarantees that $\Gamma \to \Gamma^\star$, then the ball defined in (19) becomes the origin and asymptotic stability of $\tilde{x} = 0$ is achieved, which concludes the proof.

Remark 3: As long as $\tilde{\Gamma} \neq 0$, the trajectories of the error tend to a ball of radius determined by the norm of $\tilde{\Gamma}$.

Remark 4: Note that the components of $\vec{f}_l$, corresponding to the loads, will tend to a value $\vec{f}_l^\star$; this value must correspond to an admissible behavior for the CPL, which means that it must satisfy the power flow equations that result from solving (9) under a sinusoidal regime.

This article has been accepted for publication in a future issue of this journal, but has not been fully edited. Content may change prior to final publication. Citation information: DOI 10.1109/TCSII.2018.2878188, IEEE Transactions on Circuits and Systems II: Express Briefs

IV. Test System and Simulation Results

A. Test system and simulation scenarios

The electrical configuration presented in Fig. 2 is employed as a test system to validate the mathematical model derived in this paper. All electrical parameters of the test system are presented in Table I. These electrical parameters have been taken from [16].

In the case of the photovoltaic array the maximum power available is 5 kW and its VSC is designed to support 15 kVA as maximum, which allows generating 4 kVAr of reactive power. For the motor load, we assume that its active and reactive power consumption are 6 kW and 5 kVA, respectively.

As simulation cases, we consider two extreme operating scenarios in the normal grid operation as follows: first, the stable behavior of the power grid is tested considering variations in the power generated and consumed around $\pm 20\%$ of their nominal values. Second, a short-circuit at node j with a duration of 5 cycles is simulated as extreme operative condition.

B. Simulation results

The simulation results presented in this section were carried out in MATLAB/SIMULINK software by using the Simulink/SymPowerSystem library, which allows implementing all the circuit components depicted in Fig. 2; additionally, it solves all the differential equations that result from the dynamical model via numerical approaches, such as Runge–Kutta or Backward Euler methods.

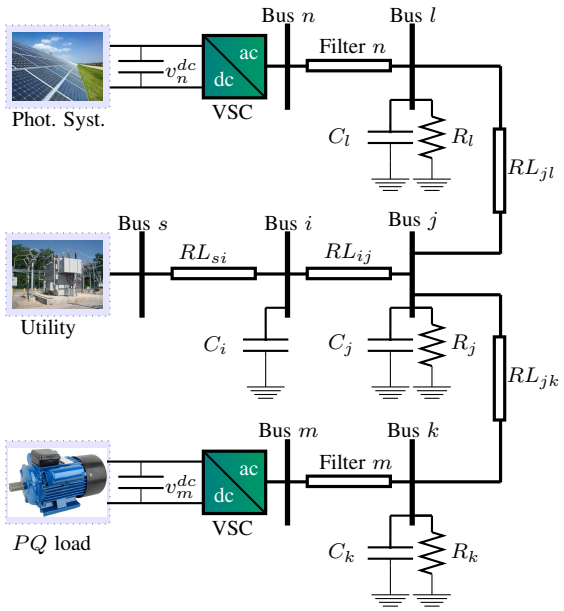

Fig. 2. Possible configuration of a generic MG [6]

TABLE I
Test System Parameters

Parameter	Value	Parameter	Value	Parameter	Value
C_i	50 μF	C_j	120 μF	C_k	200 μF
C_k	200 μF	R_{si}	20 mΩ	L_{si}	200 μH
R_{ij}	50 mΩ	L_{ij}	100 μH	R_{jk}	60 mΩ
L_{jk}	120 μH	R_{jl}	50 mΩ	L_{jl}	100 μH
R_{km}	40 mΩ	L_{km}	800 μH	R_{ln}	40 mΩ
L_{ln}	800 μH	R_j	5 Ω	$R_k = R_j$	4 Ω
f	60 Hz	V_{rms}	$\frac{380}{\sqrt{3}}$ V	V_{DC}	600 V

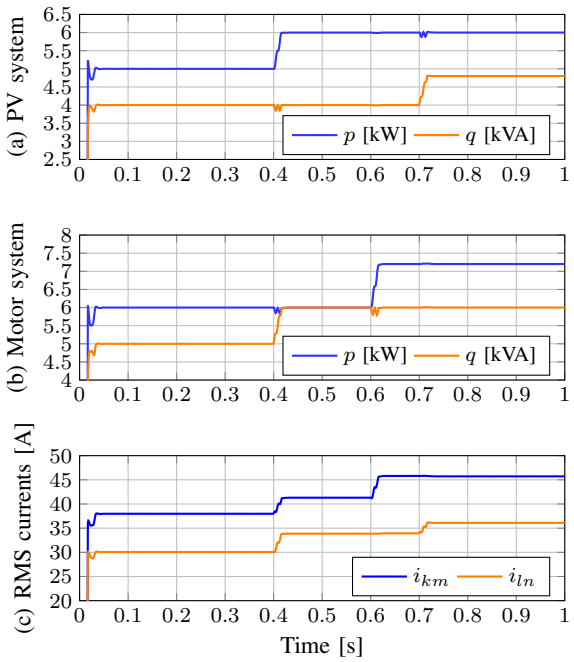

Fig. 3. Active and reactive power behavior and current RMS values: (a) photovoltaic system, (b) motor load and (c) current RMS

In the first simulation scenario, the power generation or consumption is incremented 20% respect to its nominal value as presented in Fig. 3.

Notice that when the active power in the PV system increases, some oscillation appears in the reactive power generation, this situation also occurs in the active power performance when the reactive power experiences variations in its behavior as presented in Fig. 3(a). Additionally, the motor load presents the same dynamical behavior observed for the PV system when the active or reactive power changes its operating values, as can be seen in Fig. 3(b). On the other hand, the RMS values of the filter currents show an incremental behavior (see Fig. 3(c), which is expected, since active and reactive power generation/consumption increase their values from 100% to 120%, producing important increments in the current performance due to the voltage profiles remaining near the grid voltage.

A short-circuit event is considered as second simulation scenario at node j (see Fig. 2). This short-circuit has a duration of 5 cycles of the voltage signal. In Fig. 4 the active and reactive power performance in the constant power terminals are presented as well as the voltage profile in some buses of the system.

Recall that when the short-circuit appears after about 0.4 s of simulation time, the active and reactive power generation in the PV system as well as in the motor load experience a large disturbance in terms of power behavior (see Figs. 4(a) and 4(b)); nevertheless, when the fault reaches the steady

This article has been accepted for publication in a future issue of this journal, but has not been fully edited. Content may change prior to final publication. Citation information: DOI 10.1109/TCSII.2018.2878188, IEEE Transactions on Circuits and Systems II: Express Briefs

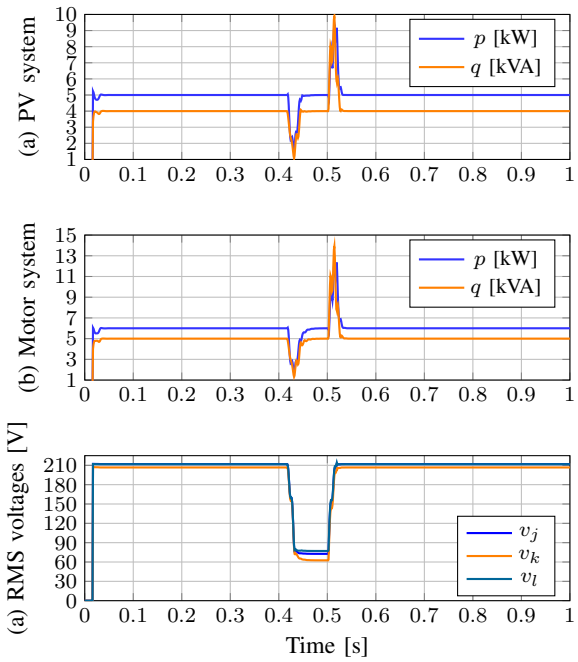

Fig. 4. Active and reactive power behavior and voltage RMS values: (a) photovoltaic system, (b) motor load and (c) voltage RMS

state, the constant power terminals continue operating under their nominal values. On the other hand, when the fault disappears, another disturbance is experienced in the constant power terminals. This occurs due to the fact that the RMS voltage in all the system nodes decreases drastically during the short-circuit event, which moves the instantaneous power behavior in the entire SP-MG.

It is important to mention that for both simulation scenarios, the SP-MG remains stable, which implies that the proposed dynamical analysis represents with a high degree of fidelity the electrical performance of the grid. Notwithstanding, this behavior is guaranteed, since the performance of the active and reactive power in the constant power terminals have a well defined behavior in terms of the power flow analysis. There are admissible trajectories for Γ for all the operating scenarios simulated. Additionally, these simulations were obtained via the iterative solution of the proposed dynamical models via the Rung–Kutta discretization methods available in MATLAB/SIMULINK software.

V. Conclusions and Future Research

In this paper, a general dynamical formulation of SP-MG is presented using a compact formulation based on the incidence matrix. This model exhibits a Hamiltonian non-autonomous structure that allows exploring its stability properties by means of Lyapunov's direct method. The stability properties are explored by employing the dynamics of the error, which permits transforming the non-autonomous model of the SP-MG into an autonomous equivalent model. Based on this transformation, the stability analysis focuses on the study of a classical regulation problem.

As future work, the approach presented in this paper can be extended to analyze three-phase microgrids. Analogously, this analysis can be made using the two-phase representation of the system applying Clarks transformation. Additionally, it would be possible to validate the dynamical model proposed in this paper via experimental tests by adding the design of controllers for constant power loads.

References

[1] S. Parhizi, H. Lotfi, A. Khodaei, and S. Bahramirad, "State of the art in research on microgrids: A review," *IEEE Access*, vol. 3, pp. 890–925, 2015.

[2] Y.-L. Ke and Y.-C. Chuang, "A novel single-stage power-factor-correction circuit with high-frequency resonant energy tank for DC-link inverters," *IEEE Trans. Circuits Syst. II*, vol. 53, no. 2, pp. 115–119, Feb 2006.

[3] A. Ortega and F. Milano, "Modeling, Simulation, and Comparison of Control Techniques for Energy Storage Systems," *IEEE Trans. Power Syst.*, vol. 32, no. 3, pp. 2445–2454, May 2017.

[4] Q. Sun, J. Zhou, J. M. Guerrero, and H. Zhang, "Hybrid Three-Phase: Single-Phase Microgrid Architecture With Power Management Capabilities," *IEEE Trans. Power Electron.*, vol. 30, no. 10, pp. 5964–5977, Oct 2015.

[5] K. Mandal and S. Banerjee, "Synchronization Phenomena in Interconnected Power Electronic Systems," *IEEE Trans. Circuits Syst. II*, vol. 63, no. 2, pp. 221–225, Feb 2016.

[6] O. D. Montoya, A. Garcés, and F. M. Serra, "DERs integration in microgrids using VSCs via proportional feedback linearization control: Supercapacitors and distributed generators," *Journal of Energy Storage*, vol. 16, pp. 250 – 258, 2018.

[7] J. W. Simpson-Porco, F. Drfler, and F. Bullo, "On Resistive Networks of Constant-Power Devices," *IEEE Trans. Circuits Syst. II*, vol. 62, no. 8, pp. 811–815, Aug 2015.

[8] D. Karimipour and F. R. Salmasi, "Stability Analysis of AC Microgrids With Constant Power Loads Based on Popov's Absolute Stability Criterion," *IEEE Trans. Circuits Syst. II Express Briefs*, vol. 62, no. 7, pp. 696–700, July 2015.

[9] S. Sanchez, R. Ortega, R. Grio, G. Bergna, and M. Molinas, "Conditions for Existence of Equilibria of Systems With Constant Power Loads," *IEEE Trans. Circuits Syst. I Regul. Pap.*, vol. 61, no. 7, pp. 2204–2211, July 2014.

[10] N. L. Soultanis, S. A. Papathanasiou, and N. D. Hatziargyriou, "A Stability Algorithm for the Dynamic Analysis of Inverter Dominated Unbalanced LV Microgrids," *IEEE Trans. Power Syst.*, vol. 22, no. 1, pp. 294–304, Feb 2007.

[11] S. Avila-Becerril, O. D. Montoya, G. Espinosa-Pérez, and A. Garcés, "Control of a Detailed Model of Microgrids from a Hamiltonian Approach," *IFAC-PapersOnLine*, vol. 51, no. 3, pp. 187–192, 2018.

[12] Y. He, H. S. Chung, C. Lai, X. Zhang, and W. Wu, "Active Cancelation of Equivalent Grid Impedance for Improving Stability and Injected Power Quality of Grid-Connected Inverter Under Variable Grid Condition," *IEEE Trans. Power Electron.*, vol. 33, no. 11, pp. 9387–9398, Nov 2018.

[13] S. Mishra, D. Pullaguram, S. A. Buragappu, and D. Ramasubramanian, "Single-phase synchronverter for a grid-connected roof top photovoltaic system," *IET Renewable Power Gener.*, vol. 10, no. 8, pp. 1187–1194, 2016.

[14] R. B. Gonzatti, S. C. Ferreira, C. H. da Silva, R. R. Pereira, L. E. B. da Silva, and G. Lambert-Torres, "Smart Impedance: A New Way to Look at Hybrid Filters," *IEEE Trans. Smart Grid*, vol. 7, no. 2, pp. 837–846, March 2016.

[15] O. D. Montoya, A. Garces, F. M. Serra, and G. Magaldi, "Apparent power control in single-phase grids using SCES devices: An IDA-PBC approach," in *2018 IEEE 9th Latin American Symposium on Circuits Systems (LASCAS)*, Feb 2018, pp. 1–4.

[16] M. M. Rezaei and J. Soltani, "A robust control strategy for a grid-connected multi-bus microgrid under unbalanced load conditions," *Int. J. Electr. Power Energy Syst.*, vol. 71, pp. 68 – 76, 2015.